

## Electronic Supplementary Information

# A Microfluidic Study of Liquid-Liquid Extraction Mediated by Carbon Dioxide

Gabriella Lestari,<sup>a</sup> Alinaghi Salari,<sup>a</sup> Milad Abolhasani,<sup>b\*</sup> and Eugenia Kumacheva<sup>a,c\*,d</sup>

<sup>a</sup> Department of Chemical Engineering, University of Toronto, 200 College Street, Toronto ON M5S 3E5, Canada

<sup>b</sup> Department of Chemical Engineering, Massachusetts Institute of Technology, 77 Massachusetts Avenue, Building 66-525, Cambridge, MA 02139, USA. E-mail: [milad@mit.edu](mailto:milad@mit.edu)

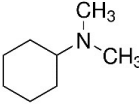
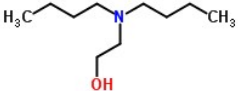

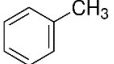
<sup>c</sup> Department of Chemistry, University of Toronto, 80 Saint George Street, Toronto, ON M5S 3H6, Canada. E-mail: [ekumachev@chem.utoronto.ca](mailto:ekumachev@chem.utoronto.ca)

<sup>d</sup> Institute of Biomaterials and Biomedical Engineering, University of Toronto, 164 College Street, Toronto ON M5S 3G9, Canada

## S1. Properties of the SHS and the liquids

All reagents were obtained from Sigma-Aldrich Canada. The chemical structures and the physical properties of the reagents are summarized in Table S1 below. Deionized water was obtained using Milli-Q<sup>®</sup> system.

**Table S1** Chemical structures and properties of the reagents<sup>1-5</sup>

Name	Linear Formula	Molecular Structure	Molecular Weight (g/mol)	Density (g/mL) at 25°C
<b>N,N-Dimethylcyclohexylamine<sup>1</sup></b>	$C_6H_{11}N(CH_3)_2$		127.23	0.849
<b>2-(Dibutylamino) ethanol<sup>2</sup></b>	$(CH_3CH_2CH_2CH_2)_2NCH_2CH_2OH$		173.30	0.86
<b>2-(Diisopropylamino) ethanol<sup>3</sup></b>	$[(CH_3)_2CH]_2NCH_2CH_2OH$		145.24	0.826
<b>Hexadecane<sup>4</sup></b>	$CH_3(CH_2)_{14}CH_3$	$CH_3(CH_2)_{14}CH_3$	226.44	0.773
<b>Toluene<sup>5</sup></b>	$C_6H_5CH_3$		92.14	0.865
<b>Water</b>	$H_2O$	$H_2O$	18.02	1.000

## S2. Experimental setup

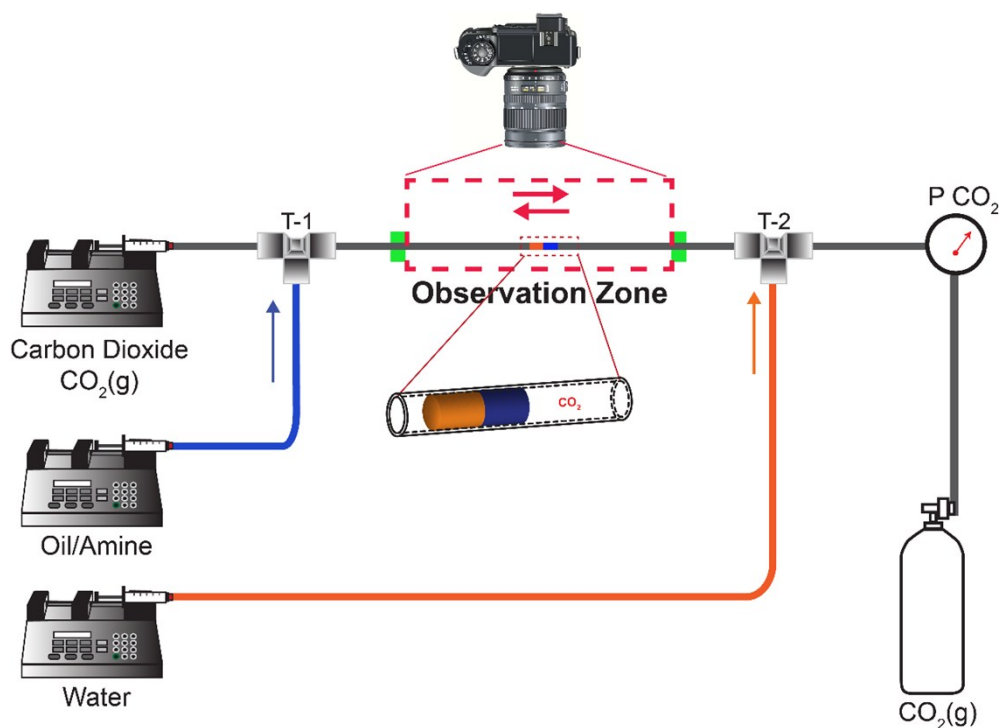
Figure S1 shows the schematic of the microfluidic (MF) platform. The experimental setup included a fluorinated ethylene propylene (FEP) tubing (1/8" OD, 1/16" ID, McMaster-Carr), a programmable syringe pump (PHD Ultra, Harvard Apparatus, U.S.A.) equipped with a gas-tight glass syringe (10 mL syringe, SGE Analytical Science), a custom-made pressurized reservoir connected to a CO<sub>2</sub> gas cylinder (99.995% purity, Linde), Tefzel® (ETFE) connectors and fittings (IDEX Health and Science), a data acquisition box (National Instrument DAQ USB-6008) and two sensors (TT Electronics, OPTEK OCB 350 Series). The sensors contained a photoresistor measuring different current values when a liquid is present or absent in the tubing. The sensors were calibrated and connected to the data acquisition box. The data acquisition box and the carrier syringe pump were connected to the computer. Using LabVIEW program, the syringe pump flow direction was controlled. As a droplet of a liquid passes the photoresistor of the sensor, the current change can be used as a cue for the LabVIEW program to change the flow direction of the syringe pump.

Prior to the experiments, the FEP tubing was purged with CO<sub>2</sub>. A 10 mL syringe was filled with CO<sub>2</sub>, and placed on the syringe pump. An aqueous droplet with the volume of 3.3-30 μL was generated at the second T-junction (T-2) and subsequently moved to the first T-junction (T-1) by changing the pressure of the carrier CO<sub>2</sub> gas syringe. Once the aqueous droplet was near T-1, the flow from the carrier CO<sub>2</sub> gas syringe was temporarily stopped. An oil droplet with the volume of 10 – 20 μL was generated at the first T-junction (T-1). The aqueous droplet and the oil droplet originally separated by a small segment of CO<sub>2</sub> gas, came into contact in the observation zone. The time, at which the two-phase adjacent oil and aqueous droplets were brought in contact, was set as the initial time (t=0). The carrier CO<sub>2</sub> gas syringe pump was started, again, to move the droplets to the observation zone (red dotted square in Fig. S1) at a low velocity of ~ 5 mm/s. Once the droplet was detected by the first sensor (green square in Fig. S1), the velocity was increased to the oscillatory flow rate (6.8 – 27.0 mm/s).

In the course of experiments, the two-phase segment oscillated between the two sensors set at a distance of 20 cm (or 30 cm, for the results of Fig. 7 in main text). The analysis of the

dimensions of the aqueous and oil droplets was performed when the segment reached its extreme positions (Figs. 2b and 2d of main text). When the two-phase droplets reached either one of the sensors, the analog output reached a logical trip lower than the calibration point, which served as a trigger in the NI LabVIEW program to change the flow direction. The back-and-forth motion of the two-phase segment continued until the LabVIEW program was manually stopped.

In the course of the experiments, a video of the oscillatory motion of the droplets was recorded (Nikon D7200). To improve the quality of visualization, either 0.1 wt% of Sudan Blue dye was added to the oil phase, or 0.05 vol% of Orange food dye was added to the aqueous phase. The video was analyzed using custom-developed MATLAB code to measure the temporal variation in droplet volume. Using the relationships below (Section S4), this information was processed to determine the fraction of amine extracted,  $n_{\text{amine, aq}}/n_{\text{amine, tot}}$ , as a function of time.

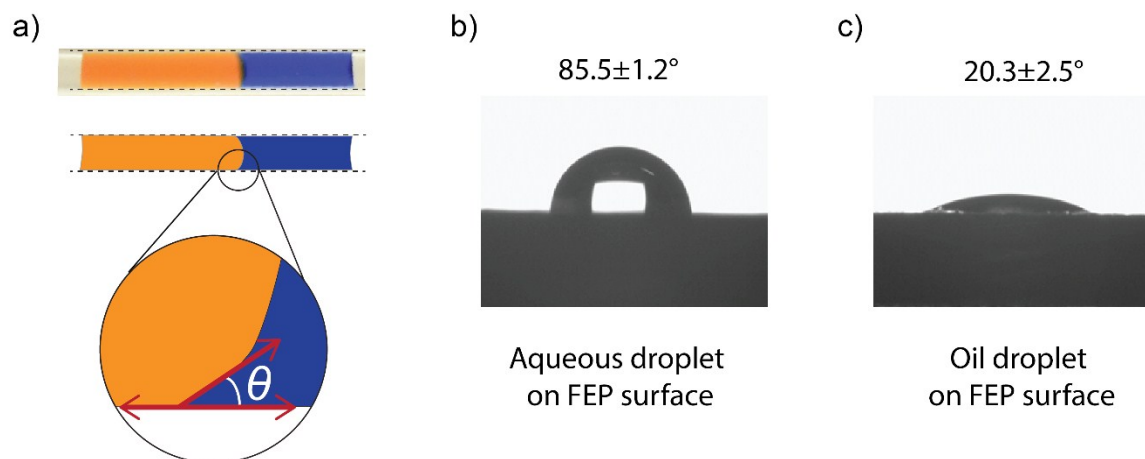


**Fig. S1** Schematic of the oscillatory microfluidic platform.

### **S3. Examination of wetting of the walls of the FEP tube reactor with the aqueous and the oil droplets**

In the course of oscillation experiments, the relative positions of the aqueous and oil droplets changed, as shown in Fig. 2 of the main text. Due to the lubricating effect of the thin oil film, as the two-phase liquid segments moved, the aqueous droplet gradually transferred to middle of the oil droplets (Fig. 2b), and then moved through the oil droplet to lead the two-phase liquid segment (Fig. 2c). This is due to the unbalanced surface tension forces at the three-phase contact line inside the fluorinated tubing material (FEP), which has a low surface energy (Fig. S2a)<sup>6</sup>.

To examine the difference between the surface energies, we measured the static contact angles of the aqueous and oil liquids on the FEP surface using Drop Shape Analyzer (DSA100, Krüss GmbH). Prior to measurements, a 1/16" thick FEP sheet (McMaster-Carr) was cleaned with ethanol and dried with N<sub>2</sub> gas. A 50 μL droplet of either deionized water (Mill-Q®) or oil (7:3 v/v of hexadecane and toluene, Sigma Aldrich) was placed on the FEP surface. Under the sessile-drop mode, using the height-width method<sup>7</sup>, the contact angles of the aqueous (Fig 2b) and the oil droplets (Fig 2c) were determined to be  $85.5 \pm 1.2^\circ$  and  $20.3 \pm 2.5^\circ$ , respectively. Thus we conclude that since the oil droplet has a lower surface energy at the interface with the FEP tubing, it remained in contact with the FEP tubing for the whole duration of the back-and-forth motion of the two-phase segment. This film provided lubrication for the aqueous droplet, which will have a more facile motion inside the FEP tubing<sup>6</sup> during the back-and-forth motion. As the aqueous droplet moved through the oil droplet, the interfacial surface area between the liquids increased (Fig S4) and additional mixing was created. Both factors favored the mass transfer of the amine.



**Fig. S2** a) Optical snapshot (top) and schematics (bottom) of the oil droplet (blue color) and aqueous droplet (orange color) wetting the interior of the FEP tube. The surface tension forces at the three-phase contact line are unbalanced (inset). b, c) Aqueous droplet (b) and oil droplet (c) positions on the FEP substrate in atmosphere of air.

#### **S4. Calibration of the density of the aqueous and oil phase as functions of SHS (amine) concentration**

The densities of the aqueous and oil liquids were determined at varying SHS (amine) concentrations in each liquid as

$$\rho_{oil} = a [A_{oil}] + \rho_{oil,0} \quad (S1)$$

$$\rho_{aq} = b [A_{aq}] + \rho_{aq,0} \quad (S2),$$

where  $\rho_{oil}$  and  $\rho_{aq}$  are the densities of the SHS-free oil and SHS-free aqueous phase in g/mL, respectively,  $[A_{oil}]$  and  $[A_{aq}]$  are the molar concentrations of the SHS in the oil and in the aqueous phase (M), respectively, and  $a$  and  $b$  are the constants obtained from the density calibration measurements of the SHS (in g/mol units).

The calibration was carried out using the same experimental setup as that used for the flow oscillation experiments. To determine the coefficient  $a$  in Eq. S1, the amine and the oil were

mixed at different volume ratios. The lengths of the droplet of amine with a particular density,  $\rho_{amine}$ , and the droplet of amine-free oil with a density,  $\rho_{o,s} = 0.886$  g/mL were measured prior to their mixing. The densities of amines used in the present work are given in Table S1. The density of the mixture of amine in oil was calculated as

$$\rho_{oil,mixture} = \frac{m_{oil,mixture}}{V_{oil,mixture}} = \frac{m_{oil\ solvent} + m_{amine}}{L_{oil,mixture} \times A_{tubing}} \quad (S3)$$

$$\rho_{oil,mixture} = \frac{L_{oil,s} \times \rho_{oil,s} \times A_{tubing} + L_{amine} \times \rho_{amine} \times A_{tubing}}{L_{oil,mixture} \times A_{tubing}} \quad (S4)$$

$$\rho_{oil,mixture} = \frac{L_{oil,s} \times \rho_{oil,s} + L_{amine} \times \rho_{amine}}{L_{o,mixture}} \quad (S5)$$

where  $A_{tubing}$  is the cross-sectional area of the tubing,  $\rho_{oil,mixture}$ ,  $\rho_{oil,s}$ , and  $\rho_{amine}$  are the density values of the one-phase oil mixture, the oil solvent, and the amine respectively, and  $L_{oil,droplet}$ ,  $L_{oil,s}$ , and  $L_{amine}$  are the measured lengths of the droplet of the amine-oil mixture at a particular amine concentration, of the oil, and of the amine, respectively. Each experiment was repeated three times.

Similarly, to obtain the coefficient  $b$  in Equation S2, a series of mixing experiment was conducted for the amine/water mixtures. Since amine in its neutral form and water are immiscible, the mixture was oscillated under  $CO_2$  atmosphere. Under these conditions the amine transformed to its hydrophilic form. In each trial, the lengths of the amine droplet of known density,  $\rho_{amine}$  and the SHS-free aqueous droplet of known density,  $\rho_{water}$  were measured individually. After mixing under  $CO_2$  atmosphere, measurements were conducted to determine the length of the droplet of the aqueous solution of protonated amine at varying amine concentrations. The density of this solution was calculated as

$$\rho_{aq,mixture} = \frac{m_{aq,mixture}}{V_{aq,mixture}} = \frac{m_{water} + m_{amine}}{L_{aq,mixture} \times A_{tubing}} \quad (S6)$$

$$\rho_{aq,mixture} = \frac{L_{water} \times \rho_{water} \times A_{tubing} + L_{amine} \times \rho_{amine} \times A_{tubing}}{L_{aq,mixture} \times A_{tubing}} \quad (S7)$$

$$\rho_{aq,mixture} = \frac{L_{water} \times \rho_{water} + L_{amine} \times \rho_{amine}}{L_{aq,mixture}} \quad (S8)$$

where  $\rho_{aq,mixture}$ ,  $\rho_{water}$ , and  $\rho_{amine}$  are the densities of the aqueous solution of protonated amine at a particular amine concentration, of the water, and of the amine respectively, and  $L_{aq,droplet}$ ,  $L_{water}$ , and  $L_{amine}$  are the measured lengths of the solution, of the water, and of the amine respectively. Each trial was repeated three times, and the amine and water were mixed at different ratios to obtain a relationship as shown in Eq. S2.

The molar concentrations of the amine in the aqueous and oil droplets at time  $t$  were determined as

$$[A_{oil}](t) = \frac{n_{amine,oil}(t)}{V_{oil}(t)} \quad (S9)$$

$$[A_{aq}](t) = \frac{n_{amine,aq}(t)}{V_{aq}(t)} \quad (S10),$$

where  $n_{amine,oil}(t)$  and  $n_{amine,aq}(t)$  are the numbers of moles of amine in the oil and aqueous phase, respectively, at time  $t$ , and  $V_{oil}(t)$  and  $V_{aq}(t)$  are the measured volumes of the oil and the aqueous droplets, respectively, at time  $t$ . The number of moles was determined as

$$n_{amine,oil}(t) = \frac{m_{amine,oil}(t)}{MW_{amine}} \quad (S11)$$

$$n_{amine,aq}(t) = \frac{m_{amine,aq}(t)}{MW_{amine}} \quad (S12),$$

where  $m_{amine,oil}(t)$  and  $m_{amine,aq}(t)$  are the masses of amine in the oil and aqueous droplets, respectively, and  $MW_{amine}$  is the molecular weight of the amine (see Table S1, Section S1). Combining Eqs. (S9) and (S11), and Eqs. (S10) and (S12), we obtained

$$[A_{oil}](t) = \frac{m_{amine,oil}(t)}{(MW_{amine}) V_{oil}(t)} \quad (S13)$$

$$[A_{aq}](t) = \frac{m_{amine,aq}(t)}{(MW_{amine}) V_{aq}(t)} \quad (S14)$$

Substitution of Eqs. (S13) and (S14) into Eqs. (S1) and (S2) yielded

$$\rho_{oil}(t) = a \frac{m_{amine,oil}(t)}{(MW_{amine}) V_{oil}(t)} + \rho_{oil,0} \quad (S15)$$

$$\rho_{aq}(t) = b \frac{m_{amine,aq}(t)}{(MW_{amine}) V_{aq}(t)} + \rho_{aq,0} \quad (S16)$$

The densities of the aqueous and oil phases at time  $t$  were determined as

$$\rho_{oil}(t) = \frac{\text{total mass in oil phase}}{\text{total volume of oil phase}} = \frac{m_{oil,solvent} + m_{amine,oil}(t)}{V_{oil}(t)} \quad (S17)$$

$$\rho_{aq}(t) = \frac{\text{total mass in aqueous phase}}{\text{total volume of aqueous phase}} = \frac{m_{water} + m_{amine,aq}(t)}{V_{aq}(t)} \quad (S18),$$

where  $m_{oil,solvent}$  is the total mass of hexadecane and toluene (g) and  $m_{water}$  is the mass of water in the aqueous phase (g). Both masses were assumed to be constant in the course of the experiments.

Combining Eqs. (S15) and (S17) yielded

$$\rho_{oil}(t) = a \frac{m_{amine,oil}(t)}{(MW_{amine}) V_{oil}(t)} + \rho_{oil,0} = \frac{m_{oil,solvent} + m_{amine,oil}(t)}{V_{oil}(t)} \quad (S19)$$

Rearrangement for the mass of amine in the oil phase at time  $t$  led to

$$m_{amine,oil}(t) = \frac{m_{oil,solvent} - \rho_{oil,0} \cdot V_{oil}(t)}{\left(\frac{a}{MW_{amine}} - 1\right)} \quad (S20)$$



Since the values of  $m_{oil,solvent}$ ,  $MW_{amine}$ ,  $a$  and  $\rho_{oil,0}$  were constant for a particular amine used, using Eq. S20 allowed us to obtain  $m_{amine,oil}(t)$ , the mass of amine in the oil phase at time  $t$ , by measuring  $V_{oil}(t)$ , that is, the volume of the oil phase, at time  $t$ .

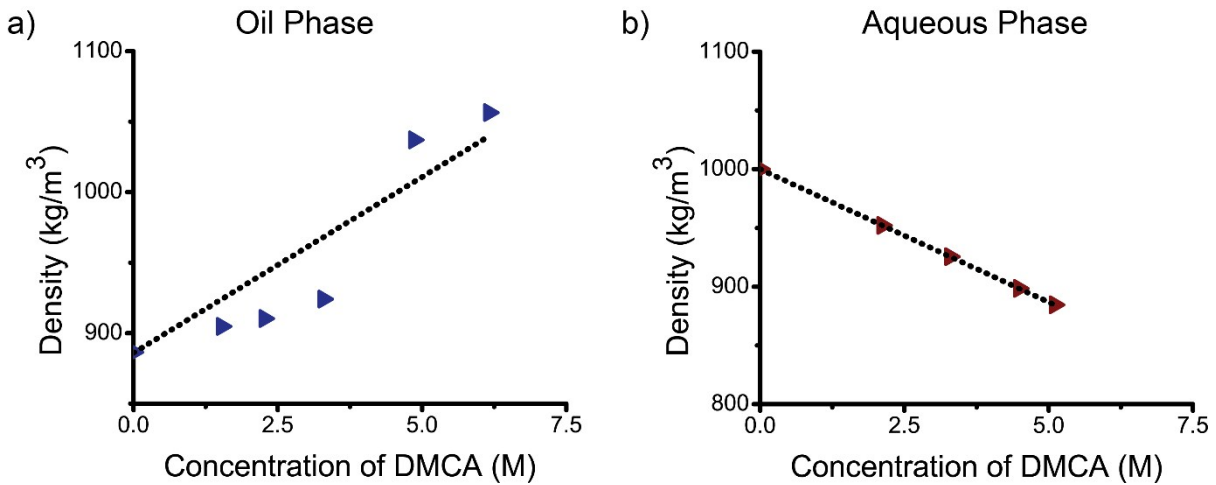
Similarly, for the aqueous phase, combining Eqs (S16) and (S18) yielded

$$\rho_{aq}(t) = b \frac{m_{amine,aq}(t)}{(MW_{amine}) V_{aq}(t)} + \rho_{aq,0} = \frac{m_{water} + m_{amine,aq}(t)}{V_{aq}(t)} \quad (S21)$$

Rearrangement of Eq. 21 for the mass of amine in the aqueous phase at time  $t$  resulted in

$$m_{amine,aq}(t) = \frac{m_{water} - \rho_{aq,0} \cdot V_{aq}(t)}{\left(\frac{b}{MW_{amine}} - 1\right)} \quad (S22)$$

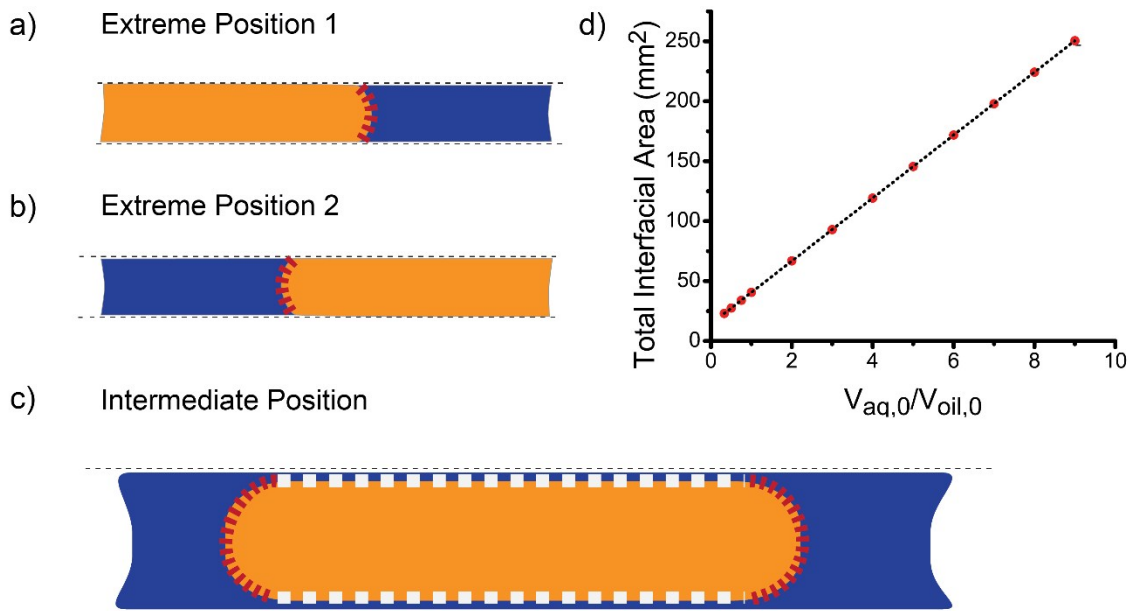
Since the values of  $m_{water}$ ,  $MW_{amine}$ ,  $a$  and  $\rho_{aq,0}$  are constant, by using Eq. S22, we obtained  $m_{amine,aq}(t)$ , the mass of the protonated amine in the aqueous phase at time  $t$ , by measuring the  $V_{aq}(t)$  at time  $t$ .



**Fig. S3** Density calibration plots of a) amine (DMCA) dissolved in the oil and b) protonated DMCA in the aqueous solution.

## S5. Interfacial Area between the oil and the aqueous phases

Figs. S4a and b show the interface between the oil and the aqueous droplets (dark-blue and orange colors, respectively) in the FEP tubing. The interface had a hemi-spherical shape, shown with the red dashed line. At the intermediate position (Fig. S4c), the total interface existed between the hemi-spherical caps and the elongated aqueous droplet and the thin film of oil (shown with the red dashed lines and the white dashed line, respectively). When the diameter of the tubing is constant, the interface between the hemi-spherical caps remains invariant, regardless of the initial ratio of  $V_{aq,0}/V_{oil,0}$ , however, as the ratio of  $V_{aq,0}/V_{oil,0}$  increases, the interfacial area corresponding to the cylindrical film increases. Figure S4d is an estimated variation of the total interfacial area at time  $t_0$  at the intermediate position for varying  $V_{aq,0}/V_{oil,0}$  for a constant  $V_{oil,0}$ . As the ratio  $V_{aq,0}/V_{oil,0}$  increases, the total interfacial area undergoes a linear increase.



**Fig. S4** (a, b) The hemi-spherical interface between the oil (dark-blue) and aqueous (orange) droplets (shown with a red dashed line) at two extreme droplet positions, (c) The interface between the oil (dark-blue) and aqueous (orange) droplets at an intermediate position of the two-phase segment. The interface is formed between the hemi-spherical caps of the oil and

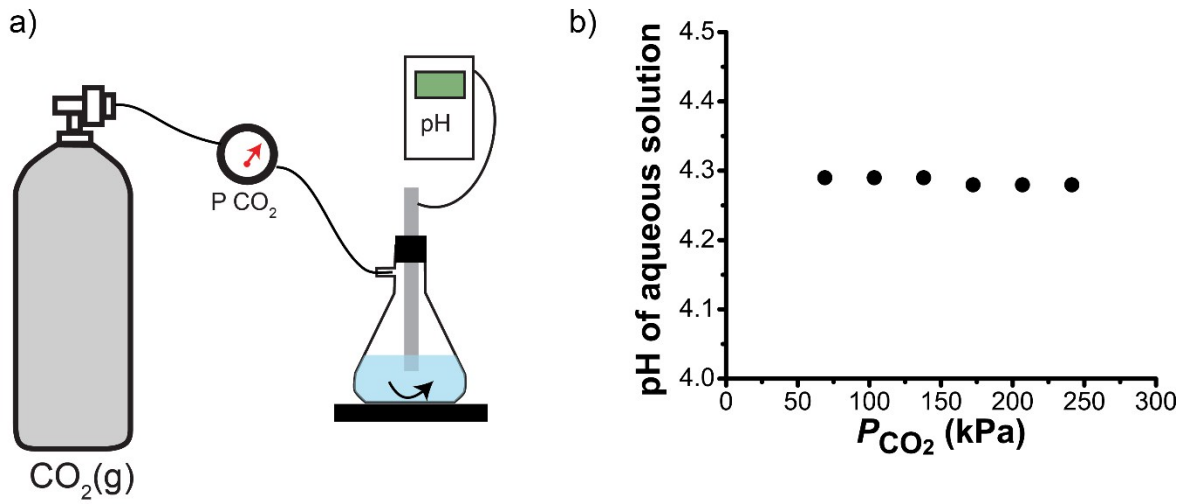
aqueous phases (red dashed line) and the cylindrical oil film engulfing the aqueous droplet (shown with a white dashed line), (d) The estimated relationship between the total interfacial area between the aqueous and oil droplets at time  $t_0=0$  and the initial ratio of the volumes of the aqueous and oil phases at  $V_{oil,0}=\text{const}$ .

During the extraction process, the volume of the aqueous droplet gradually increased. The increase in the volumetric ratio of aqueous phase to oil phase resulted in an increase of the total available interfacial area available for mass transfer. This dynamic variation resulted in a non-linear relationship between the extraction time and the ratio  $V_{aq,0}/V_{oil,0}$  (Fig. 4c, main text).

### **S6. The effect of the applied CO<sub>2</sub> pressure on the pH of aqueous solution**

Figure S5a shows the experimental setup used to measure the value of pH of deionized water (Milli-Q®) at varying pressure of CO<sub>2</sub> gas in bulk system. A 25-mL Büchner flask containing deionized water was connected to the CO<sub>2</sub> gas supply. The use of magnetic stirring ensured a uniform distribution of dissolved CO<sub>2</sub> and formed carbonic acid throughout the flask. CO<sub>2</sub> gas was bubbled into the deionized water for at least, 15 min. Then, a pH electrode (VWR) connected to a pH meter (EcoMet P25, Istek) was placed through a hole made in a rubber stop to ensure a pressurized system. Readings of the pH of the aqueous solution were obtained for the CO<sub>2</sub> pressure in the range of 20-200 kPa.

The value of pH of the aqueous solution saturated with CO<sub>2</sub> gas remained at  $4.28 \pm 0.01$  after 15 min experiment. The result indicated that for the range of operating pressure studied, a significant reduction in extraction time  $t_{\text{extr}}$  (>400% reduction when  $PCO_2$  was increased from 69 to 241 kPa) resulted from the higher concentration of CO<sub>2</sub> dissolved into the water, and not from the change in pH of the solution.



**Fig. S5** (a) Experimental setup used for the measurements of pH of an aqueous solution saturated with CO<sub>2</sub> under different CO<sub>2</sub> pressures, (b) Variation in pH of the aqueous solution under varying  $P_{\text{CO}_2}$ . The CO<sub>2</sub> gas was bubbled into the deionized water for at least, 15 min.

## S6. Calculation of dimensionless numbers

The dimensionless Reynolds number characterizing the ratio of the inertial and viscous forces and the dimensionless Weber number, characterizing the ratio of inertia to surface tension forces were calculated as shown in Eqs. S23 and S24, respectively.

Reynolds number ( $Re$ ):

$$Re = \frac{\rho U D}{\mu} \quad (\text{S23})$$

Weber number ( $We$ ):

$$We = \frac{\rho U^2 D}{\sigma} \quad (\text{S24})$$

where  $\rho$ ,  $\mu$ ,  $\sigma$ ,  $U$ , and  $D$  are the density of the fluid, the viscosity of the fluid, the surface tension of the fluid, the average velocity of fluid, and the inner diameter of the tube respectively.

In order to identify the flow regime inside the mixing droplets, the highest  $Re$  number had to be determined. As water has a higher density and a lower viscosity than the oil mixture, the value of  $Re$  of the aqueous phase is higher than the value of  $Re$  of the oil phase. Therefore, the value of  $Re$  number associated with the aqueous phase was calculated. Using  $U = 27 \text{ mm/s}$ ,  $D = 1.59 \text{ mm}$ ,  $\rho = 1000 \text{ kg/m}^3$ , and  $\mu = 1 \text{ mPa}\cdot\text{s}$ , we calculated the value of  $Re$  number at room temperature to be  $Re \approx 42$ . For smooth circular tubes, the critical value of  $Re$ , below which the flow is laminar, is approximately  $2300^{8-10}$ , and thus the assumption of laminar flow used in our work was valid. Nevertheless, the back-and-forth motion of the two-phase water-oil segment significantly improved the mixing through recirculation.

As the oil droplet mostly consists of hexadecane (70 vol%), we calculated  $We$  number for hexadecane, corresponding to the upper limit of the oscillation velocity, above which the oil droplet breaks into smaller droplets. For hexadecane, using  $U = 27 \text{ mm/s}$ ,  $D = 1.59 \text{ mm}$ ,  $\rho = 770 \text{ kg/m}^3$ , and  $\sigma = 28.12 \text{ mN/m}$ , the value of  $We$  was 0.032.

## S7. Calculation of extraction time and distribution ratio

Extraction time was calculated from the exponential fitting of the curve of  $n_{amine,aq}/n_{amine,t}$  with respect to time. The time required to complete extraction was defined as the time when 95% of the extraction has taken place. The fit equation for the curve of  $n_{amine,aq}/n_{amine,t}$  vs.  $t$  is

$y = A(1 - e^{-\frac{t}{T}})$ . The time required to complete extraction,  $t_{ext}$ , was defined when  $y = 0.95A$ .

Therefore, it can also be expressed as  $t_{ext} = T \ln 0.05$ . The value of  $T$  was obtained from the fitting of the curve using the user-defined function on OriginPro.

Distribution ratio was calculated as the total molar concentration of DMCA in the aqueous phase to its total molar concentration in the oil.

$$D = \frac{\text{total molar concentration of DMCA in aqueous phase}}{\text{total molar concentration of DMCA in oil phase}} \quad (S25)$$

$$D = \frac{\frac{n_{amine,aq}}{V_{aq}}}{\frac{n_{amine,oil}}{V_{oil}}} = \frac{\frac{n_{amine,aq}}{n_{amine,tot}} \times \frac{1}{V_{aq}}}{\frac{n_{amine,oil}}{n_{amine,tot}} \times \frac{1}{V_{oil}}} \quad (S26)$$

$$D = \frac{\frac{n_{amine,aq}}{n_{amine,tot}}}{\frac{n_{amine,oil}}{n_{amine,tot}}} \times \frac{V_{oil}}{V_{aq}} \quad (S27)$$

## References

1. *N,N-Dimethylcyclohexylamine*,  
<http://www.sigmaaldrich.com/catalog/product/aldrich/290629?lang=en&region=CA>.
2. *2-(Dibutylamino)ethanol*,  
<http://www.sigmaaldrich.com/catalog/product/aldrich/550035?lang=en&region=CA>.
3. *2-(Diisopropylamino)ethanol*,  
<http://www.sigmaaldrich.com/catalog/product/aldrich/471488?lang=en&region=CA>.
4. *Hexadecane*,  
<http://www.sigmaaldrich.com/catalog/product/sial/h6703?lang=en&region=CA>.
5. *Toluene*,  
<http://www.sigmaaldrich.com/catalog/product/sial/244511?lang=en&region=CA>.
6. M. Abolhasani, C. W. Coley and K. F. Jensen, *Anal Chem*, 2015, **87**, 11130-11136.
7. K. GmbH, *Height-width method*, <http://www.kruss.de/services/education-theory/glossary/height-width-method/>, Accessed 09 March, 2016.
8. N. Rott, *Annu Rev Fluid Mech*, 1990, **22**, 1-11.
9. E. Bobok, *Fluid mechanics for petroleum engineers*, Elsevier, 1993.
10. K. Avila, D. Moxey, A. de Lozar, M. Avila, D. Barkley and B. Hof, *Science*, 2011, **333**, 192-196.